Identification of Lasso Peptide Topologies Using Native nESI-Trapped Ion Mobility Spectrometry – Mass Spectrometry

Kevin Jeanne Dit Fouque,[†] Javier Moreno,[†] Julian D. Hegemann,[‡] Séverine Zirah,[§] Sylvie Rebuffat,[§] and Francisco Fernandez-Lima *[,†]

[†] Department of Chemistry and Biochemistry, Florida International University, Miami, FL 33199, USA.

[‡] Department of Chemistry, University of Illinois, Urbana-Champaign, IL 61801, USA.

[§] Muséum National d'Histoire Naturelle, Sorbonne Universités, Laboratoire MCAM, 75005 Paris, France.

ABSTRACT: Lasso peptides are a fascinating class of bioactive ribosomal natural products characterized by a mechanically interlocked topology. In contrast to their branched-cyclic forms, lasso peptides have higher stability and have become a scaffold for drug development. However, the identification and separation of lasso peptides from their unthreaded topoisomers (branched-cyclic peptides) is analytically challenging since the higher stability is based solely on differences in their tertiary structures. In the present work, a fast and effective workflow is proposed for the separation and identification of lasso from branched cyclic peptides based on differences in their mobility space under native nESI - trapped ion mobility spectrometry – mass spectrometry (nESI-TIMS-MS). The high mobility resolving power (*R*) of TIMS resulted in the separation of lasso and branched-cyclic topoisomers (*R* up to 250, 150 needed on average). The advantages of alkali metalation reagents (e.g. Na, K and Cs salts) as a way to increase the analytical power of TIMS is demonstrated for topoisomers with similar mobilities as protonated species, efficiently turning the metal ion adduction into additional separation dimensions.

Natural products have long played important roles in drug development. Among them, ribosomally synthesized and post-translationally modified peptides (RiPPs) present a broad structural diversity, typically restricting conformational flexibility to allow better target recognition and to increase chemical, physical and proteolytic stability augmenting chemical functionality.[1,2] Lasso peptides are a structurally fascinating class of RiPPs exhibiting enzyme inhibitory, receptor antagonistic, antimicrobial or antiviral properties.[2,3] All lasso peptides are characterized by their unique mechanically interlocked topology in which the C-terminal tail is threaded through and trapped within an N-terminal macrolactam ring generated by an isopeptide bond between the alpha-amino group of the residue at position 1 and the side chain carboxyl group of a glutamate or aspartate residue at position 7, 8 or 9 (Figure S1).[2-4] Strong sterical constraints, , mediated by bulky side chains above and below the ring, named plugs, and/or by disulfide bonds, stabilize the lasso structure leading to a compact [1]rotaxane type structure. As a consequence of their compact and interlocked structures, lasso peptides often display strong resistance against chemical and proteolytic degradation as well as, in many cases, thermally-induced unthreading.[5-8]

Since the discovery of this class of RiPPs, more than 40 lasso peptides were found in actinobacteria, proteobacteria, and firmicutes.[2,4,9] Their size ranges from 13 to 24 residues, and they are classified depending on the absence (class II) or presence (class I and class III) of disulfide bonds that can further stabilize the lasso structure (Figure S1). Many lasso peptides were discovered through genome mining approaches and isolation and characterization of new representatives of this RiPP family is still an active area of research.[6,10-14] The extraordinary mechanically interlocked topology of lasso peptides, together with their panel of biological activities makes them a scaffold for drug development.[15,16] It is worth mentioning that the lasso structure, required for the biological activities of lasso peptides, constitute a source of inspiration for bioengineering and chemical synthesis.[5, 17] Recent studies have reported structural lasso mimics including a self-entanglement strategy using a pH-sensitive lasso molecular switch,[18] and the chemical synthesis of peptide-based [1]rotaxane using synthesis of [2]rotaxane followed by chemoselective ligation.[19] One limitation to the activity of lasso peptides is unthreading of the C-terminal tail, a trend reported for certain lasso peptides, yielding their corresponding branched-cyclic topoisomers.[6-8,20] Thus, the discovery and design of new lasso peptides as potential drug candidates requires high throughput analytical tools capable of distinguishing them from their unthreaded branched-cyclic topoisomers.

Liquid chromatography is regularly used as a means to differentiate the two topoisomers, especially when following thermally-induced unthreading or enzymatic digestion with carboxypeptidases.[2, 5-8, 10] Generally, the lasso peptide shows no or much less truncation than the branched-cyclic analog that arises from heat-associated unthreading.

Traditional condensed-phase separations are nowadays increasingly complemented or replaced by faster, gas-phase separations (e.g., ion mobility spectrometry – mass spectrometry, IMS-MS). IMS-MS has gained broad

acceptance in a variety of bioanalytical applications (e.g., small molecules,[21] lipidomics,[22] proteomics,[23] and structural biology[24]) thanks to the high speed, higher selectivity and increased peak capacity.

A few recent studies report the use of traveling wave IMS (TWIMS) for the characterization of lasso peptides. The modest resolving power (R) of the TWIMS with dynamic field (R ~ 30 - 50), implemented in the Synapt G2 instrument (Waters),[25] has allowed only limited (if any) separation between lasso and branched-cyclic topoisomers.[26,27] Attempts to increase the TWIMS resolution have been reported using oligomers,[28,29] shift reagents,[30] metalation,[28,31] or increase of the charge states in view of slower diffusion.[32,33] For example, the use of sulfolane as a supercharging reagent,[34] permitted the differentiation of lasso and branched-cyclic topoisomers at high charge states, which was not observed for lower charged species (Figure S2).[26,27,35]

The push for higher resolution and sensitivity has led to the developments of various forms of IMS devices, that can be typically classified as scanning (e.g., FAIMS,[36] DMA,[37] and transverse modulation IMS[38]) or dispersive (e.g., drift-tube IMS,[39] periodic focusing drift tube IMS,[40] TWIMS,[41] overtone mobility IMS,[42] cyclic TWIMS,[43] and SLIMS[44]). In particular, the recent introduction of trapped IMS (TIMS) and its integration with MS analyzers,[45-50] has found multiple applications in analytical workflows with high mobility resolving power (R up to ~400) in a compact geometry.[51] TIMS-MS devices have proven useful for rapid separation and structural elucidation of biomolecules,[50,52-61] for screening[52] and targeted[48,50] analysis of complex mixtures, tracking isomerization kinetics,[53-55] characterizing the conformational spaces of peptides,[62] separation of D-amino acid containing peptides,[63] DNA,[56] proteins,[64-66] and macromolecular complexes in native and denatured states.[67]

In the present work, two class I, ten class II and one class III lasso peptides (Table 1) were studied using native nESI-TIMS MS for the first time. Branched-cyclic analogs that were available for five class II lasso peptides were used for comparison. In the following discussion, we demonstrate the TIMS capability for high throughput screening of peptide topoisomers in native starting solvent conditions.

EXPERIMENTAL SECTION

Materials and Reagents

Microcin J25 was produced by cultivation of *Escherichia coli* MC4100 harboring the plasmid pTUC202,[68] as previously described.[69] Anantin,[70,71] BI-32169,[72] capistruin,[73] and siamycin I, [74,75] were produced by their respective native hosts, as reported elsewhere (Table S1). Caulonodin I-III,[6] sphingonodin I,[6] syanodin I,[6] and xanthomonin I-II,[76] were produced heterologously in *E. coli* BL21 (DE3) under controlled conditions as previously described (Table S1). Sviceucin was produced heterologously in *Streptomyces coelicolor* transformed with the cosmid p4H7, as described elsewhere.[77] The experimental conditions are listed in detail in the Supporting Information (Table S1). The purification procedures of lasso peptides are reported elsewhere.[35]

The branched-cyclic peptide of syanodin I was obtained by heating the lasso peptide at 95°C for 3 h and was subsequently purified by reversed-phase HPLC. For capistruin, caulonodin III, microcin J25 and sphingonodin I, which are heat stable lasso peptides, topoisomeric variants were obtained by solid-phase synthesis from Genepep (St Jean de Védas, France). The carbonate salts of Na, K, and Cs were purchased from Acros Organics (New Jersey, USA). The peptides were dissolved in 10 mM NH_4Ac (native conditions) to 5 µM with or without 70 µM of a carbonate salt. The instrument was initially calibrated using the Tuning Mix[47] from Agilent (Santa Clara, CA).

Table 1. Sequence and molecular mass of all analyzed lasso peptides. The macrolactam rings, loops, plugs and C-terminal tails are highlighted in green, blue, red and orange, respectively. The proposed plugs of lasso peptides, for which the 3D structures are still not elucidated, are colored in purple. Lasso peptides for which a corresponding branched-cyclic peptide was produced are underlined.

Peptide	Sequence	Molecular mass (Da)	Class
Sviceucin	CVWGGDCTDFLGCGTAWICV	2084.41	Class I
Siamycin I	CLGVGSCNDFAGCGYAIVCFW	2163.51	Class I
Xanthomonin II	GGPLAGEEMGGITT	1271.40	Class II
Syanodin I	GISGGTVDAPAGQGLAG	1409.50	Class II
Xanthomonin I	GGPLAGEEIGGFNVPG	1452.57	Class II
Sphingonodin I	GPGGITGDVGLGENNFG	1542.61	Class II
Caulonodin I	GDVLNAPEPGIGREPTG	1660.78	Class II
Caulonodin II	GDVLFAPEPGVGRPPMG	1677.92	Class II
Caulonodin III	GQIYDHPEVGIGAYGCE	1789.92	Class II
Anantin	GFIGWGNDIFGHYSGDF	1870.97	Class II
Capistruin	GTPGFQTPDARVISRFGFN	2049.25	Class II
Microcin J25	GGAGHVPEYFVGIGTPISFYG	2107.32	Class II
BI-32169	GLPWGCPSDIPGWNTPWAC	2037.29	Class III

TIMS-MS Experiments

We employed a custom nESI-TIMS unit coupled to an Impact Q-TOF mass spectrometer (Bruker, Billerica, MA).[45,46] The TIMS unit is run by custom software in LabView (National Instruments) synchronized with the MS platform controls.[46] Sample aliquots (10 μL) were loaded in a pulled-tip capillary biased at 700-1200 V to the MS inlet. TIMS separation depends on the gas flow velocity (v_g), elution voltage ($V_{elution}$), ramp time (t_{ramp}) and base voltage (V_{out}).[45,78] The mobility, K, is defined by:

$$K = \frac{v_g}{E} = \frac{A}{(V_{elution} - V_{out})} \quad (1)$$

The mobility calibration constant A was determined using known reduced mobilities of Tuning Mix components. The resolving power (R) and resolution (r) are defined as $R = \Omega/w$ and $r = 1.18*(\Omega_2-\Omega_1)/(w_1+w_2)$, where w is the full peak width at half maximum (FWHM). The scan rate ($Sr=\Delta V_{ramp}/t_{ramp}$) was optimized to discriminate the two topoisomers; differences in the IMS bands (e.g., broadening) mainly arises from unresolved populations illustrated by differences the R values during the same acquisition conditions. The buffer gas was N_2 at ambient temperature (T) with v_g set by the pressure difference between the funnel entrance (P1 = 2.6 mbar) and exit (P2 = 1.1 mbar, Figure S3). An rf voltage of 200 V_{pp} at 880 kHz was applied to all electrodes. Ions were softly transferred and injected into the TIMS analyser section injection to avoid collisional induced activation. The measured mobilities were converted into collision cross sections (CCS, Å²) using the Mason-Schamp equation:

$$\Omega = \frac{(18\pi)^{1/2}}{16}\frac{q}{(k_B T)^{1/2}}\left(\frac{1}{m}+\frac{1}{M}\right)^{1/2}\frac{1}{N}\times\frac{1}{K} \quad (2)$$

where q is the ion charge, k_B is the Boltzmann constant, N is the gas number density, m is the ion mass, and M is the gas molecule mass.[78]

RESULTS AND DISCUSSION

Native nESI-TIMS-MS Analysis of Lasso Peptides

Inspection of the MS spectra of the lasso peptides analyzed using native nESI mostly showed a single charge state species, (i.e., $[M+2H]^{2+}$) in contrast to higher charge states observed using conventional ESI in denaturing conditions (e.g., $[M+2H]^{2+}$ and $[M+3H]^{3+}$).[26] This difference in the charge state distribution is significant, since lasso peptides exposed to a supercharging reagent,[34] did not provide major changes (e.g., only an additional charge state ($[M+4H]^{4+}$) was observed). Typical, high resolution trapped IMS spectra corresponding to the doubly protonated species of individual lasso peptide standards are presented in Figure 1 and the measured CCS and R metrics are listed in Table S2. The high resolution IMS profiles exhibited a remarkably large variety of IMS bands, which was not expected according to the relatively compact lasso topology. Previous TWIMS experiments usually showed a single broad arrival time distribution for the doubly protonated species.[26,27] By contrast, when the same peptides are analyzed using high resolution TIMS, a higher number of IMS bands and features can be observed providing additional information on the conformational space of lasso peptides. We interpret the higher conformational diversity observed during

native nESI-TIMS as a consequence of the soft conditions that lead to the observation of multiple conformational motifs and the high resolving power of the TIMS analyzer. The presence of multiple IMS bands also suggests the possibility to stabilize the tertiary structure using several combinations of intramolecular interactions. For example, different protonation schemes can lead to charge-driven intramolecular interactions and stabilization of the conformational motif that will define a particular lasso topology. Different from traditional peptides (e.g., linear peptides), the threading of the macrolactam ring by the C-terminal tail region (Figure 1), and potential disulfide bonds can add supplementary restraints to the conformational motifs of the lasso peptides. For example, class II lasso peptides (without disulfide bonds) are mainly mechanically constrained by the plugs with additional intramolecular interactions between the flexible C-terminal tail (highlighted in orange in Figure 1) and the macrolactam ring (green).

Moreover, closer inspection of the IMS profiles suggests that the amino acid composition of the C-terminal tail can impose significant folding restrictions to the lasso topology. For example, one protonation scheme could preserve a relatively tight folding of the flexible C-terminal tail around the macrolactam ring, leading to a compact conformation. This folding could be stabilized though charge solvation,[27] and/or by the formation of intramolecular interactions implying hydrogen bonds between the macrolactam ring and the penetrating C-terminal tail.[79,80] An alternative scheme could include protonation of the C-terminal tail leading to coulombic repulsion which unfolds the flexible C-terminal tail and promotes a more extended conformation. These two scenarios can be correlated to the relative abundances of the IMS bands with the length and amino acid composition of the C-terminal tail. For example, lasso peptides with long C-terminal tails (>4 residues) result in higher abundance of the most extended conformation (e.g., syanodin I, xanthomonin I, caulonodin I, and caulonodin II, Figure 1), while short C-terminal tails (<5 residues) result in higher abundance of the IMS bands corresponding to the most compact conformation (e.g., xanthomonin II, sphingonodin I, caulonodin III, anantin,

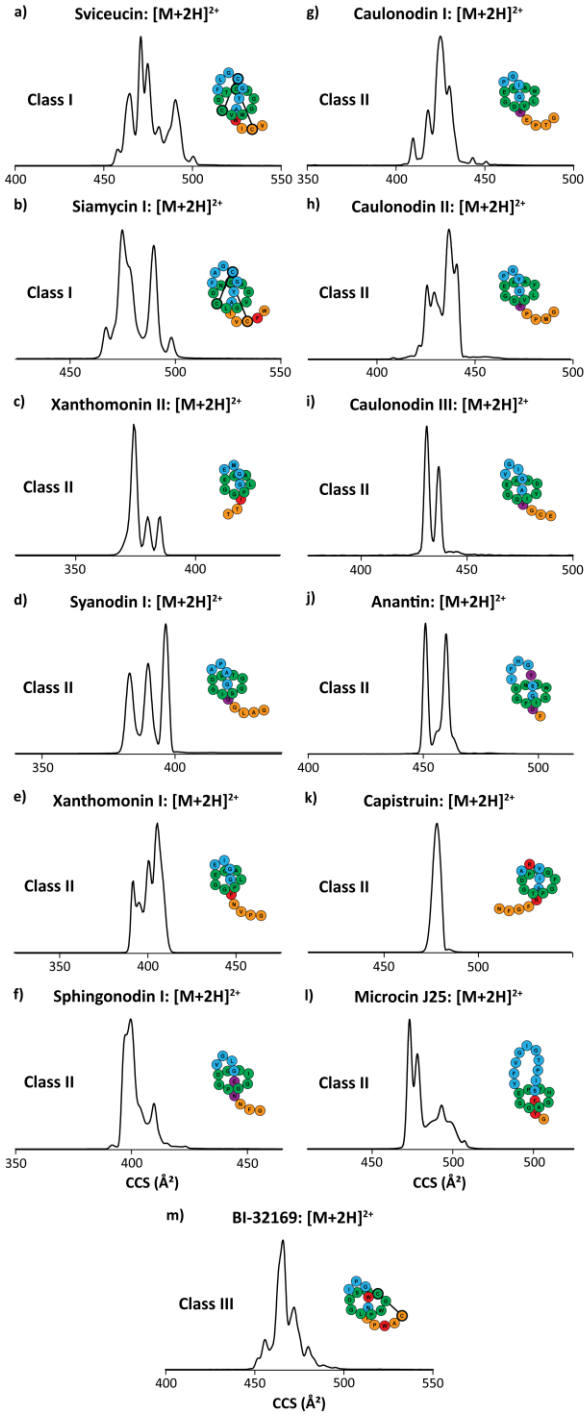

Figure 1. Typical TIMS spectra of a) sviceucin, b) siamycin I, c) xanthomonin II, d) syanodin I, e) xanthomonin I, f) sphingonodin I, g) caulonodin I, h) caulonodin II, i) caulonodin III, j) anantin, k) capistruin, l) microcin J25 and m) BI-32169 for [M+2H]2+ ions. Schemes highlight the macrolactam rings in green, the loops in blue, the plugs in red/purple and the C-terminal tails in orange. The disulfide bonds are represented by black lines.

and microcin J25 Figure 1). The single IMS band observed for capistruin (Figure 1k) can be a consequence of the charge solvation on Arg15 by the carbonyl groups of Phe18 and Asn19, and by possible hydrogen bond formation between the C-terminal carboxyl group and backbone carbonyls near Arg11 leading to a tight folding of the C-terminal tail around the macrolactam ring.[27,79]

In addition to the scenario described, the class I/III lasso peptides are additionally stabilized by disulfide bonds preventing the unfolding of the C-terminal tail. Nevertheless, inspection of the IMS profiles of sviceucin (Figure 1a), siamycin I (Figure 1b) and BI-32169 (Figure 1m) shows multiple IMS bands that cover a relatively broad CCS region as compared to the class II lasso peptides. This suggests that the disulfide bonds can prevent the peptides for collapsing to more compact populations. In this context, the observed diversity may rather originate from competition between different protonation schemes favoring higher abundance of compact/extended conformation depending on the length of the loop and C-terminal regions.

High throughput screening of peptide topoisomers using nESI-TIMS-MS

The potential of native nESI-TIMS-MS as a high throughput screening tool for peptide topoisomers was evaluated for capistruin, caulonodin III, microcin J25, sphingonodin I and syanodin I, with their corresponding branched-cyclic topoisomers (Figure 2). While the lasso and their corresponding branched-cyclic topoisomers share the same amino acid sequence, they can be differentiated based on their tertiary structures and fragmentation profiles. In a recent paper, a combination of electron transfer dissociation (ETD) and collision induced dissociation (CID) fragmentation was used to distinguish the two topologies.[81] CID experiments yielded lasso-specific fragments, where the N-terminal macrolactam ring and a part of the C-terminal tail remain interlocked through the steric hindrance provided by the side chains of bulky residues, only for class II lasso peptides in which the loop was strictly longer than four residues. In addition, ETD experiments of lasso peptides specifically showed larger extents of hydrogen migration located in the loop region, leading to the formation of c_i•/z_j' from c_i'/z_j• fragments, for all class II lasso peptides, regardless of the size of the loop. The combination of these two techniques appears powerful for the characterization of both lasso and branched-cyclic topoisomers, but they are time-consuming and have limited application for the case of mixtures (Table S4).

Figure 2 show that by using fast scan rates (*Sr* = 0.3 – 0.56 V/ms, Table S3), high mobility resolving power (*R* of ~ 90 – 200, with an average of ~ 130 required) was achieved, which in turn permitted the observation of several

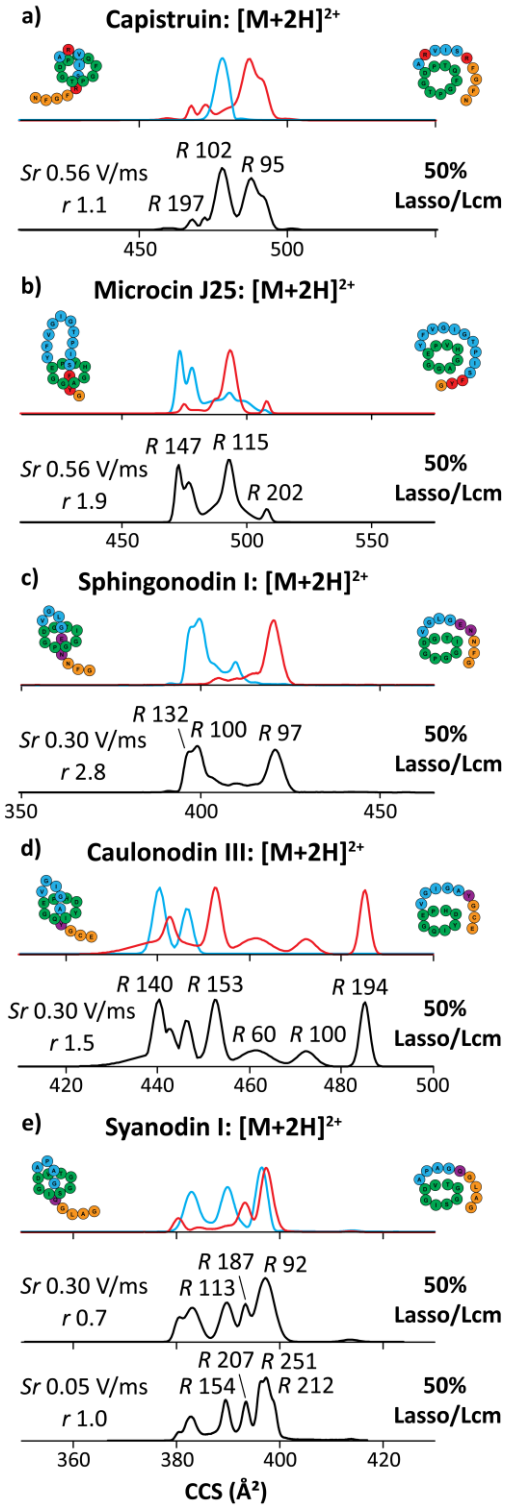

Figure 2. Typical high resolution IMS spectra for $[M+2H]^{2+}$ ions of (a) capistruin, (b) microcin J25, (c) sphingonodin I, (d) caulonodin III and (e) syanodin I (blue traces) with their branched-cyclic topoisomers (red traces) using nESI-TIMS-MS. The *R*, *r*, and scan rate values are given.

signature features in the IMS domain (i.e., fingerprint CCS profiles). The fast scan rates resulted in baseline separation of the sphingonodin I (r = 2.8), microcin J25 (r = 1.9) and caulonodin III (r = 1.5), near baseline resolution of the capistruin (r = 1.1) and limited separation for the syanodin I (r = 0.7, Figure 2) topoisomers. In the case of syanodin I, slow scan rates (Sr = 0.05 V/ms, Table S3) are needed to resolve the topoisomers, leading to resolving powers of R ~ 120 - 250 (with an average of ~190 required) and near baseline resolution (r ~ 1.0) (Figure 2e and Table S2). While previous attempts using TWIMS separations have not resulted in the separation of the topoisomers without the addition of chemical reagents,[26,27] the high resolving power of the TIMS analyzer provided baseline analytical separation of the five lasso peptide topoisomers (Table S2). In addition to the high resolving power, the relative ($\Delta\Omega_r$) and absolute ($\Delta\Omega$) CCS differences can provide accurate measurement allowing clear topoisomeric differentiation: 1.8% (9 Å²) for capistruin, 1.6% (7 Å²) for caulonodin III, 3.0% (15 Å²) for microcin J25, 4.8% (20 Å²) for sphingonodin I and 0.8% (3 Å²) for syanodin I (Table S2). Inspection of the examples shown in Figure 2 show that TIMS is effective for the differentiation of the lasso and branched-cyclic topologies with at least $\Delta\Omega_r$ ~ 0.8% differences. For all the lasso and branched-cyclic peptides investigated, the most intense conformation of the doubly protonated branched-cyclic peptides had higher CCS, confirming the concept that the C-terminal part of branched-cyclic peptides are more expanded than for lasso peptides, where the C-terminal tail is threaded. This trend was more or less pronounced according to the length of the flexible C-terminal tail of the lasso peptides. In fact, a short C-terminal tail resulted in higher CCS difference while a long C-terminal tail resulted in closer CCS difference with the branched-cyclic peptide.

Enhancing Topoisomer Separations Using Metalation

A common approach to increase the analytical power of IMS techniques is the use of metalation.[28,31,82,83] For example, nESI-TIMS analysis of syanodin I does not provide a clear separation of the main conformation of the doubly protonated lasso and branched-cyclic topoisomers ($\Delta\Omega_r$ ~ 0.25% (1.2 Å²) and r ~ 0.4, Figure 2e), despite the high resolving power of the TIMS analyzer. Alternatively, the conformational motifs of the metalated species generally differ to their protonated molecules, as the metal ions may bind to different sites and/or coordinate differently because of their chemical differences, potentially leading to effective IMS separation.[84] The effect of alkali metals on the TIMS separation of lasso and branched-cyclic topoisomers is illustrated in Figures 3 and S4 for $[M+2X]^{2+}$, where X = H, Na, K, and Cs. Inspection of Figure 3 shows that for all cases, the metal ion cationized species resulted in higher IMS resolution

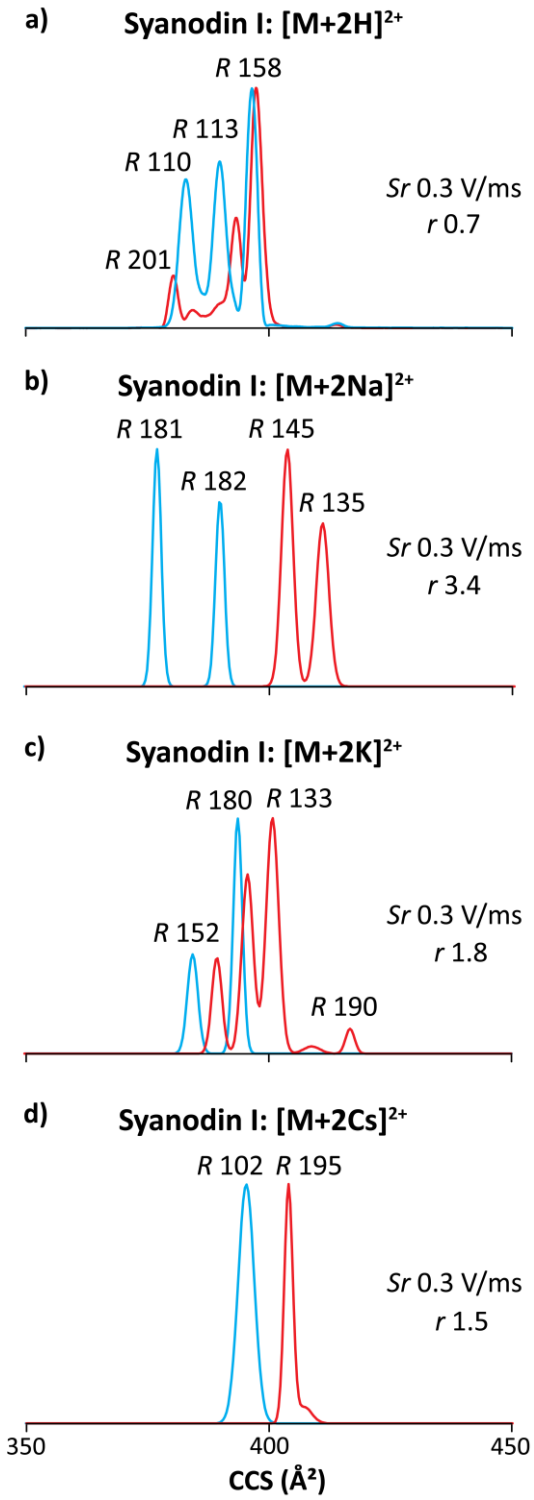

Figure 3. Typical high resolution IMS spectra for syanodin I (blue traces) and its branched-cyclic (red traces) topoisomers cationized by (a) protonated, (b) sodiated, (c) potassiated, and (d) cesiated species using nESI-TIMS-MS. The R, r, and Sr values are given.

(r, by at least a factor of 2) between the lasso and branched-cyclic topoisomers compared to the IMS resolution achieved using the protonated species, enabling their separation at fast scan rates (Tables S2 and S3). The most pronounced difference was observed for $[M+2Na]^{2+}$, where the relative mobility difference was 3.5% (14 Å²) with a resolution of $r \sim 3.4$ between the syanodin I topoisomers. For caulonodin III, the sodiated species did not improve the resolution ($r \sim 1.4$) but the potassiated ($r \sim 2.6$) and cesiated ($r \sim 1.8$) species allowed to baseline resolved the two topoisomers (Figure S4e-h). In the case of the well separated protonated sphingonodin I ($r \sim 2.8$), the metal ion cationized species did not improve the resolution (r comparable for $[M+2Na]^{2+}$ species) between the lasso and branched-cyclic topoisomers (Figure S4a-d).

The mobility resolution between the lasso and the branched-cyclic topoisomers tends to decrease as the ionic radius of the alkali metal increases. For example, the mobility resolution between the lasso and the branched-cyclic topoisomers decreases from ~ 3.4 to ~ 1.5 for syanodin I (Figure 3b-d), and ~ 2.7 to ~ 2.0 for sphingonodin I (Figure S4b-d). For caulonodin III, this trend is only observed for the $[M+2K]^{2+}$ and $[M+2Cs]^{2+}$, as the resolution using the $[M+2Na]^{2+}$ ($r \sim 1.4$) is comparable for $[M+2H]^{2+}$ ($r \sim 1.5$), with a decrease in resolution of $r \sim 2.6$ to ~ 1.8, respectively (Figure S4e-h). In addition, different numbers of IMS bands are observed as a function of the metal ion size for the same charge state in the two topoisomers. For example, while the IMS profile typically consisted of multiple IMS bands, the IMS profile of the cesiated species consists of a single IMS band for each species (Figures 3d, S4d and S4h) permitted to clearly discriminate both lasso and branched-cyclic topologies. This example illustrates the potential of metalation as an additional analytical dimension for high throughput screening of peptide topoisomers using high resolution native nESI-TIMS in good agreement with previous metalation experiments using other IMS variants.[28,31,82,83]

CONCLUSIONS

The potential of native nESI-TIMS-MS for high throughput screening of peptide topoisomers was illustrated for the first time for lasso peptides and their branched-cyclic analogs. In particular, the high resolving power ($R \sim 90$ - 250) of the TIMS analyzer provided a "fingerprint" of the conformational space (e.g., multiple IMS bands) and baseline separation of the topoisomers. The analysis of five topoisomer mixtures in native starting solvent conditions showed that CCS differences of 0.8 - 3% are sufficient for effective separation of the topoisomers. For all the peptides considered, the most intense conformation of the doubly protonated branched-cyclic peptides had higher CCS, confirming the concept that the C-terminal part of branched-cyclic peptides are more unfolded than for the mechanically interlocked lasso peptides. The effect of the C-terminal chain length and amino acid composition on the IMS profile was also discussed.

The added analytical advantages of metalation to the nESI-TIMS-MS workflow were illustrated in the case of syanodin I topoisomers, where the differences in the IMS profiles can be enlarged by using alkali metal adducts (e.g., 2Na, 2K and 2Cs). Different IMS profiles for the topoisomers are obtained as a function of the metal ions for the same charge state, suggesting that the size of the metal ion plays an important role on the conformational space and type of intramolecular interactions that stabilize the conformational motifs. [31,85]

We demonstrate the performance of high resolution TIMS, as compared to previous TWIMS implementation and CID/ETD techniques, for the identification of lasso and branched-cyclic topologies based on their absolute mobilities (Table S4). However, one limitation of TIMS-MS remains the assignment of the plug residues responsible for the stabilization of the threaded C-terminal tail. Since ExD processes appear to be powerful in the lasso and branched-cyclic topoisomer discrimination and assignment of the plugs residues, we anticipate that further instrumental developments of TIMS and their coupling with ExD will allow further advancements on the global lasso analyses in biological systems.

ASSOCIATED CONTENT

Supporting Information

General classification criteria for lasso peptides, CCS range observed for multiply protonated species using TWIMS, scheme of the TIMS cell, TIMS spectra for cationized sphingonodin I and its branched-cyclic topoisomers, conditions for the production of lasso peptides, Tables of the measured separation parameters and potential/weakness of the reported techniques. This material is available free of charge via the Internet at http://pubs.acs.org.

AUTHOR INFORMATION

Corresponding Author

fernandf@fiu.edu

Author Contributions

The manuscript was written through contributions of all authors. All authors have given approval to the final version of the manuscript.

Notes

The authors declare no competing financial interest.

ACKNOWLEDGEMENTS

This work was supported by a NSF CAREER (CHE-1654274), with co-funding from the Division of Molecular and Cellular Biosciences to FFL. The authors would also like to acknowledge the helpful discussions and technical support from Dr. Mark E. Ridgeway and Dr. Melvin A. Park from Bruker Daltonics Inc. during the fabrication of the custom-built TIMS-TOF MS instrument.

REFERENCES

(1) Arnison, P. G.; Bibb, M. J.; Bierbaum, G.; Bowers, A. A.; Bugni, T. S.; Bulaj, G.; Camarero, J. A.; Campopiano, D. J.; Challis, G. L.; Clardy, J.; Cotter, P. D.; Craik, D. J.; Dawson, M.; Dittmann, E.; Donadio, S.; Dorrestein, P. C.; Entian, K. D.; Fischbach, M. A.; Garavelli, J. S.; Goransson, U.; Gruber, C. W.; Haft, D. H.; Hemscheidt, T. K.; Hertweck, C.; Hill, C.; Horswill, A. R.; Jaspars, M.; Kelly, W. L.; Klinman, J. P.; Kuipers, O. P.; Link, A. J.; Liu, W.;

Marahiel, M. A.; Mitchell, D. A.; Moll, G. N.; Moore, B. S.; Muller, R.; Nair, S. K.; Nes, I. F.; Norris, G. E.; Olivera, B. M.; Onaka, H.; Patchett, M. L.; Piel, J.; Reaney, M. J.; Rebuffat, S.; Ross, R. P.; Sahl, H. G.; Schmidt, E. W.; Selsted, M. E.; Severinov, K.; Shen, B.; Sivonen, K.; Smith, L.; Stein, T.; Sussmuth, R. D.; Tagg, J. R.; Tang, G. L.; Truman, A. W.; Vederas, J. C.; Walsh, C. T.; Walton, J. D.; Wenzel, S. C.; Willey, J. M.; van der Donk, W. A. *Nat. Prod. Rep.* **2013**, *30*, 108-160.

(2) Hegemann, J. D.; Zimmermann, M.; Xie, X.; Marahiel, M. A. *Acc. Chem. Res.* **2015**, *48*, 1909-1919.

(3) Maksimov, M. O.; Pan, S. J.; James Link, A. *Nat. Prod. Rep.* **2012**, *29*, 996-1006.

(4) Li, Y.; Zirah, S.; Rebuffat, S. *Lasso Peptides: Bacterial Strategies to Make and Maintain Bioactive Entangled Scaffolds*; Springer: New York, 2015.

(5) Ducasse, R.; Yan, K. P.; Goulard, C.; Blond, A.; Li, Y.; Lescop, E.; Guittet, E.; Rebuffat, S.; Zirah, S. *ChemBioChem* **2012**, *13*, 371-380.

(6) Hegemann, J. D.; Zimmermann, M.; Zhu, S.; Klug, D.; Marahiel, M. A. *Biopolymers* **2013**, *100*, 527-542.

(7) Zimmermann, M.; Hegemann, J. D.; Xie, X.; Marahiel, M. A. *Chem. Biol.* **2013**, *20*, 558-569.

(8) Hegemann, J. D.; Fage, C. D.; Zhu, S.; Harms, K.; Di Leva, F. S.; Novellino, E.; Marinelli, L.; Marahiel, M. A. *Mol. Biosyst.* **2016**, *12*, 1106-1109.

(9) Zhu, S.; Hegemann, J. D.; Fage, C. D.; Zimmermann, M.; Xie, X.; Linne, U.; Marahiel, M. A. *J. Biol. Chem.* **2016**, *291*, 13662-13678.

(10) Hegemann, J. D.; Zimmermann, M.; Xie, X.; Marahiel, M. A. *J. Am. Chem. Soc.* **2013**, *135*, 210-222.

(11) Maksimov, M. O.; Link, A. J. *J. Ind. Microbiol. Biotechnol.* **2014**, *41*, 333-344.

(12) Maksimov, M. O.; Pelczer, I.; Link, A. J. *Proc. Natl. Acad. Sci. USA* **2012**, *109*, 15223-15228.

(13) Kersten, R. D.; Yang, Y. L.; Xu, Y.; Cimermancic, P.; Nam, S. J.; Fenical, W.; Fischbach, M. A.; Moore, B. S.; Dorrestein, P. C. *Nat. Chem. Biol.* **2011**, *7*, 794-802.

(14) Tietz, J. I.; Schwalen, C. J.; Patel, P. S.; Maxson, T.; Blair, P. M.; Tai, H. C.; Zakai, U. I.; Mitchell, D. A. *Nat. Chem. Biol.* **2017**, *13*, 470-478.

(15) Knappe, T. A.; Manzenrieder, F.; Mas-Moruno, C.; Linne, U.; Sasse, F.; Kessler, H.; Xie, X.; Marahiel, M. A. *Angew. Chem. Int. Ed. Engl.* **2011**, *50*, 8714-8717.

(16) Hegemann, J. D.; De Simone, M.; Zimmermann, M.; Knappe, T. A.; Xie, X.; Di Leva, F. S.; Marinelli, L.; Novellino, E.; Zahler, S.; Kessler, H.; Marahiel, M. A. *J. Med. Chem.* **2014**, *57*, 5829-5834.

(17) Lear, S.; Munshi, T.; Hudson, A. S.; Hatton, C.; Clardy, J.; Mosely, J. A.; Bull, T. J.; Sit, C. S.; Cobb, S. L. *Org. Biomol. Chem.* **2016**, *14*, 4534-4541.

(18) Clavel, C.; Fournel-Marotte, K.; Coutrot, F. *Molecules* **2013**, *18*, 11553-11575.

(19) Saito, F.; Bode, J. W. *Chem. Sci.* **2017**, *8*, 2878-2884.

(20) Knappe, T. A.; Linne, U.; Robbel, L.; Marahiel, M. A. *Chem. Biol.* **2009**, *16*, 1290-1298.

(21) Lapthorn, C.; Pullen, F.; Chowdhry, B. Z. *Mass Spectrom. Rev.* **2013**, *32*, 43-71.

(22) Paglia, G.; Kliman, M.; Claude, E.; Geromanos, S.; Astarita, G. *Anal. Bioanal. Chem.* **2015**, *407*, 4995-5007.

(23) Zhong, Y.; Hyung, S. J.; Ruotolo, B. T. *Expert Rev. Proteomics* **2012**, *9*, 47-58.

(24) Lanucara, F.; Holman, S. W.; Gray, C. J.; Eyers, C. E. *Nat. Chem.* **2014**, *6*, 281-294.

(25) Giles, K.; Williams, J. P.; Campuzano, I. *Rapid Commun. Mass Spectrom.* **2011**, *25*, 1559-1566.

(26) Jeanne Dit Fouque, K.; Afonso, C.; Zirah, S.; Hegemann, J. D.; Zimmermann, M.; Marahiel, M. A.; Rebuffat, S.; Lavanant, H. *Anal. Chem.* **2015**, *87*, 1166-1172.

(27) Jeanne Dit Fouque, K.; Lavanant, H.; Zirah, S.; Lemoine, J.; Rebuffat, S.; Tabet, J. C.; Kulesza, A.; Afonso, C.; Dugourd, P.; Chirot, F. *Rapid Commun. Mass Spectrom.* **2015**, *29*, 1411-1419.

(28) Domalain, V.; Tognetti, V.; Hubert-Roux, M.; Lange, C. M.; Joubert, L.; Baudoux, J.; Rouden, J.; Afonso, C. *J. Am. Soc. Mass Spectrom.* **2013**, *24*, 1437-1445.

(29) Pang, X.; Jia, C.; Chen, Z.; Li, L. *J. Am. Soc. Mass Spectrom.* **2017**, *28*, 110-118.

(30) Yang, H.; Shi, L.; Zhuang, X.; Su, R.; Wan, D.; Song, F.; Li, J.; Liu, S. *Sci. Rep.* **2016**, *6*, 28079.

(31) Flick, T. G.; Campuzano, I. D.; Bartberger, M. D. *Anal. Chem.* **2015**, *87*, 3300-3307.

(32) Shvartsburg, A. A.; Smith, R. D. *Anal. Chem.* **2008**, *80*, 9689-9699.

(33) Watts, P.; Wilders, A. *Int. J. Mass Spectrom. Ion Proc.* **1992**, *112*, 179-190.

(34) Lomeli, S. H.; Peng, I. X.; Yin, S.; Loo, R. R.; Loo, J. A. *J. Am. Soc. Mass Spectrom.* **2010**, *21*, 127-131.

(35) Fouque, K. J.; Lavanant, H.; Zirah, S.; Hegemann, J. D.; Zimmermann, M.; Marahiel, M. A.; Rebuffat, S.; Afonso, C. *J. Am. Soc. Mass Spectrom.* **2017**, *28*, 315-322.

(36) Shvartsburg, A. A.; Li, F.; Tang, K.; Smith, R. D. *Anal. Chem.* **2006**, *78*, 3706-3714.

(37) de la Mora, J. F.; Ude, S.; Thomson, B. A. *Biotechnol. J.* **2006**, *1*, 988-997.

(38) Vidal-de-Miguel, G.; Macia, M.; Cuevas, J. *Anal. Chem.* **2012**, *84*, 7831-7837.

(39) Tang, K.; Shvartsburg, A. A.; Lee, H. N.; Prior, D. C.; Buschbach, M. A.; Li, F.; Tolmachev, A. V.; Anderson, G. A.; Smith, R. D. *Anal. Chem.* **2005**, *77*, 3330-3339.

(40) Blase, R. C.; Silveira, J. A.; Gillig, K. J.; Gamage, C. M.; Russell, D. H. *Int. J. Mass Spectrom.* **2011**, *301*, 166-173.

(41) Giles, K.; Pringle, S. D.; Worthington, K. R.; Little, D.; Wildgoose, J. L.; Bateman, R. H. *Rapid Commun. Mass Spectrom.* **2004**, *18*, 2401-2414.

(42) Kurulugama, R. T.; Nachtigall, F. M.; Lee, S.; Valentine, S. J.; Clemmer, D. E. *J. Am. Soc. Mass Spectrom.* **2009**, *20*, 729-737.

(43) Giles, K.; Wildgoose, J. L.; Pringle, S.; Garside, J.; Carney, P.; Nixon, P.; Langridge, D. J. *In 62nd Annual ASMS Conference on Mass Spectrometry and Allied Topics*, Baltimore, MD, June 15-19, **2014**.

(44) Tolmachev, A. V.; Webb, I. K.; Ibrahim, Y. M.; Garimella, S. V.; Zhang, X.; Anderson, G. A.; Smith, R. D. *Anal. Chem.* **2014**, *86*, 9162-9168.

(45) Fernandez-Lima, F. A.; Kaplan, D. A.; Suetering, J.; Park, M. A. *Int. J. Ion Mobil. Spectrom.* **2011**, *14*, 93-98.

(46) Fernandez-Lima, F. A.; Kaplan, D. A.; Park, M. A. *Rev. Sci. Instr.* **2011**, *82*, 126106.

(47) Hernandez, D. R.; Debord, J. D.; Ridgeway, M. E.; Kaplan, D. A.; Park, M. A.; Fernandez-Lima, F. *Analyst* **2014**, *139*, 1913-1921.

(48) Benigni, P.; Thompson, C. J.; Ridgeway, M. E.; Park, M. A.; Fernandez-Lima, F. *Anal. Chem.* **2015**, *87*, 4321-4325.

(49) Benigni, P.; Fernandez-Lima, F. *Anal. Chem.* **2016**, *88*, 7404-7412.

(50) Benigni, P.; Sandoval, K.; Thompson, C. J.; Ridgeway, M. E.; Park, M. A.; Gardinali, P.; Fernandez-Lima, F. *Environ. Sci. Technol.* **2017**, *51*, 5978-5988.

(51) Adams, K. J.; Montero, D.; Aga, D.; Fernandez-Lima, F. *Int. J. Ion Mobil. Spectrom.* **2016**, *19*, 69-76.

(52) Castellanos, A.; Benigni, P.; Hernandez, D. R.; DeBord, J. D.; Ridgeway, M. E.; Park, M. A.; Fernandez-Lima, F. A. *Anal. Meth.* **2014**, *6*, 9328-9332.

(53) Schenk, E. R.; Mendez, V.; Landrum, J. T.; Ridgeway, M. E.; Park, M. A.; Fernandez-Lima, F. *Anal. Chem.* **2014**, *86*, 2019-2024.

(54) Molano-Arevalo, J. C.; Hernandez, D. R.; Gonzalez, W. G.; Miksovska, J.; Ridgeway, M. E.; Park, M. A.; Fernandez-Lima, F. *Anal. Chem.* **2014**, *86*, 10223-10230.

(55) McKenzie-Coe, A.; DeBord, J. D.; Ridgeway, M.; Park, M.; Eiceman, G.; Fernandez-Lima, F. *Analyst* **2015**, *140*, 5692-5699.

(56) Garabedian, A.; Butcher, D.; Lippens, J. L.; Miksovska, J.; Chapagain, P. P.; Fabris, D.; Ridgeway, M. E.; Park, M. A.; Fernandez-Lima, F. *Phys. Chem. Chem. Phys.* **2016**, *18*, 26691-26702.

(57) Meier, F.; Beck, S.; Grassl, N.; Lubeck, M.; Park, M. A.; Raether, O.; Mann, M. *J. Proteome Res.* **2015**, *14*, 5378-5387.

(58) Pu, Y.; Ridgeway, M. E.; Glaskin, R. S.; Park, M. A.; Costello, C. E.; Lin, C. *Anal. Chem.* **2016**, *88*, 3440-3443.

(59) Liu, F. C.; Kirk, S. R.; Bleiholder, C. *Analyst* **2016**, *141*, 3722-3730.

(60) Garabedian, A.; Benigni, P.; Ramirez, C. E.; Baker, E. S.; Liu, T.; Smith, R. D.; Fernandez-Lima, F. *J. Am. Soc. Mass Spectrom.* **2017**, DOI: 10.1007/s13361-017-1787-8.

(61) Molano-Arevalo, J. C.; Gonzalez, W.; Jeanne dit fouque, K.; Miksovska, J.; Maitre, P.; Fernandez-Lima, F. *Phys. Chem. Chem. Phys.* **2018**, *20*, 7043-7052.

(62) Schenk, E. R.; Ridgeway, M. E.; Park, M. A.; Leng, F.; Fernandez-Lima, F. *Anal. Chem.* **2014**, *86*, 1210-1214.

(63) Jeanne Dit Fouque, K.; Garabedian, A.; Porter, J.; Baird, M.; Pang, X.; Williams, T. D.; Li, L.; Shvartsburg, A.; Fernandez-Lima, F. *Anal. Chem.* **2017**, *89*, 11787-11794.

(64) Schenk, E. R.; Almeida, R.; Miksovska, J.; Ridgeway, M. E.; Park, M. A.; Fernandez-Lima, F. *J. Am. Soc. Mass Spectrom.* **2015**, *26*, 555-563.

(65) Molano-Arevalo, J. C.; Jeanne Dit Fouque, K.; Pham, K.; Miksovska, J.; Ridgeway, M. E.; Park, M. A.; Fernandez-Lima, F. *Anal. Chem.* **2017**, *89*, 8757-8765.

(66) Garabedian, A.; Baird, M. A.; Porter, J.; Jeanne Dit Fouque, K.; Shliaha, P. V.; Jensen, O. N.; Williams, T. D.; Fernandez-Lima, F.; Shvartsburg, A. A. *Anal. Chem.* **2018**, *90*, 2918-2925.

(67) Benigni, P.; Marin, R.; Molano-Arevalo, J. C.; Garabedian, A.; Wolff, J. J.; Ridgeway, M. E.; Park, M. A.; Fernandez-Lima, F. *Int. J. Ion Mobil. Spectrom.* **2016**, *19*, 95-104.

(68) Solbiati, J. O.; Ciaccio, M.; Farias, R. N.; Gonzalez-Pastor, J. E.; Moreno, F.; Salomon, R. A. *J. Bacteriol.* **1999**, *181*, 2659-2662.

(69) Salomon, R. A.; Farias, R. N. *J. Bacteriol.* **1992**, *174*, 7428-7435.

(70) Weber, W.; Fischli, W.; Hochuli, E.; Kupfer, E.; Weibel, E. K. *J. Antibiot.* **1991**, *44*, 164-171.

(71) Wyss, D. F.; Lahm, H. W.; Manneberg, M.; Labhardt, A. M. *J. Antibiot.* **1991**, *44*, 172-180.

(72) Knappe, T. A.; Linne, U.; Xie, X.; Marahiel, M. A. *FEBS Lett.* **2010**, *584*, 785-789.

(73) Knappe, T. A.; Linne, U.; Zirah, S.; Rebuffat, S.; Xie, X.; Marahiel, M. A. *J. Am. Chem. Soc.* **2008**, *130*, 11446-11454.

(74) Yano, K.; Toki, S.; Nakanishi, S.; Ochiai, K.; Ando, K.; Yoshida, M.; Matsuda, Y.; Yamasaki, M. *Bioorg. Med. Chem.* **1996**, *4*, 115-120.

(75) Katahira, R.; Yamasaki, M.; Matsuda, Y.; Yoshida, M. *Bioorg. Med. Chem.* **1996**, *4*, 121-129.

(76) Hegemann, J. D.; Zimmermann, M.; Zhu, S.; Steuber, H.; Harms, K.; Xie, X.; Marahiel, M. A. *Angew. Chem. Int. Ed. Engl.* **2014**, *53*, 2230-2234.

(77) Li, Y.; Ducasse, R.; Zirah, S.; Blond, A.; Goulard, C.; Lescop, E.; Giraud, C.; Hartke, A.; Guittet, E.; Pernodet, J. L.; Rebuffat, S. *ACS Chem. Biol.* **2015**, *10*, 2641-2649.

(78) McDaniel, E. W.; Mason, E. A. *Mobility and diffusion of ions in gases*; John Wiley and Sons, Inc., New York: New York, 1973, p 381.

(79) Jeanne Dit Fouque, K.; Lavanant, H.; Zirah, S.; Steinmetz, V.; Rebuffat, S.; Maitre, P.; Afonso, C. *J. Phys. Chem. A* **2016**, *120*, 3810-3816.

(80) Rosengren, K. J.; Clark, R. J.; Daly, N. L.; Goeransson, U.; Jones, A.; Craik, D. J. *J. Am. Chem. Soc.* **2003**, *125*, 12464-12474.

(81) Jeanne Dit Fouque, K.; Lavanant, H.; Zirah, S.; Hegemann, J. D.; Fage, C. D.; Marahiel, M. A.; Rebuffat, S.; Afonso, C. *Analyst* **2018**, *143*, 1157-1170.

(82) Leavell, M. D.; Gaucher, S. P.; Leary, J. A.; Taraszka, J. A.; Clemmer, D. E. *J. Am. Soc. Mass Spectrom.* **2002**, *13*, 284-293.

(83) Clowers, B. H.; Hill, H. H., Jr. *J. Mass Spectrom.* **2006**, *41*, 339-351.

(84) Dilger, J. M.; Valentine, S. J.; Glover, M. S.; Ewing, M. A.; Clemmer, D. E. *Int. J. Mass Spectrom.* **2012**, *330*, 35-45.

(85) Domalain, V.; Hubert-Roux, M.; Lange, C. M.; Baudoux, J.; Rouden, J.; Afonso, C. *J. Mass Spectrom.* **2014**, *49*, 423-427.